Research Article

For reprint orders, please contact: reprints@futuremedicine.com

Nanomedicine

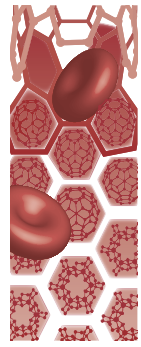

Nanoformulated paclitaxel and AZD9291 synergistically eradicate non-small-cell lung cancers *in vivo*

Xin-shuai Wang[1], Li Zhang[1], Xiaocen Li[2], De-jiu Kong[1], Xiao-chen Hu[1], Xue-zhen Ding[1], Jun-qiang Yang[1], Meng-qi Zhao[1], Yixuan He[2], Kit S Lam[2], She-gan Gao[1], Tzu-yin Lin*[,3] & Yuanpei Li**[,2]

[1]Henan Key Laboratory of Cancer Epigenetics, Cancer Hospital, The First Affiliated Hospital, College of Clinical Medicine, Medical College of Henan, University of Science & Technology, Luoyang 471003, China

[2]Department of Biochemistry & Molecular Medicine, University of California Davis, Sacramento, CA 95817, USA

[3]Department of Internal Medicine, School of Medicine, University of California Davis, Sacramento, CA 95817, USA

*Author for correspondence: tylin@ucdavis.edu

**Author for correspondence: lypli@ucdavis.edu

Aim: This study aims to develop new nanoformulations of EGFR T790M targeted inhibitor AZD9291 and paclitaxel (PTX) for combination therapy of lung cancer. **Materials & methods:** We prepared and characterized PTX- and AZD9291-loaded disulfide cross-linking micelles (DCMs), and evaluate their combination effect and toxicity *in vitro* and in lung cancer-bearing mice. **Results:** Drug-loaded DCMs were relatively small in size, and possessed glutathione-responsive drug release. The combination of PTX–DCMs and AZD92921–DCMs exhibited strong synergistic effects in both cell line and *in vivo* without additional toxicity. Molecular studies demonstrated the synergistic modification in both IKB-α/NF-κB/Bcl-2 and EGFR/Akt pathways. **Conclusion:** The combination of DCM-loaded AZD9291 and PTX could potentially offer more effective and less toxicity treatment options for lung cancer patients.

First draft submitted: 23 November 2017; Accepted for publication: 13 March 2018; Published online: 6 June 2018

Keywords: AZD9291 • EGFR inhibitor • NSCLC • paclitaxel

Lung cancer is the leading cause of cancer-related mortality for both men and women worldwide, with approximately 85% of patients suffering from non-small-cell lung cancer (NSCLC) [1]. For the most patients with advanced lung cancers, the standard of care is chemotherapy; however, the toxicity induced by chemotherapy greatly limited the use of chemotherapy in clinical settings [1–3]. Moreover, although chemotherapy provides the relief of cancer symptoms and improves the quality of life, it could only marginally prolong patient survival for a few months at best in patients with late-stage cancers [4,5]. Thus, there is clearly an unmet clinical need and exploring new effective integrated treatment methods to improve the quality of life and prolong the survival time of advanced NSCLC patients is required.

The important chemotherapeutics used against lung cancers are typically lipophilic and require higher doses for administration and/or surfactant-based solubilization to improve the systemic drug availability. Due to their nontargeting nature, chemotherapeutics also attack normal tissues leading to adverse effects [6]. Paclitaxel (PTX) is an antimicrotubule agent and is frequently used to treat lung cancers. The main drawbacks of PTX are toxicity, poor solubility, low tumor selectivity and fast body elimination. Adverse reactions include allergy, bone marrow suppression, neural toxicity, cardiotoxicity, gastrointestinal reaction and hair loss [7]. The above toxicities remarkably lessen the life quality of patients and limit the therapeutic dose of chemotherapy.

The discovery of genetic diversity in NSCLC has demonstrated the power of precision medicine in genetically defined tumors. About 10–40% of NSCLC patients harbor activating mutations of *EGFR* and were proven to be a valid cancer target [8,9]. The common *EGFR* mutation includes a deletion in exon 19 and/or a point mutation in exon 21 and response well with the first generation of EGFR TKIs, such as gefitinib, erlotinib and afatinib [10–12]. Unfortunately, most patients eventually developed resistance after development of a second mutation,

Future Medicine

amplification of MET, epithelial–mesenchymal transition and small cell histologic transformation [13–15], resulting disease progression [16,17]. Particularly, T790M mutation occurred in 60% of *EGFR*-mutant NSCLC patients after TKI treatment [13]. Several third generations of *EGFR*-TKIs, such as Osimertinib (AZD9291), were developed to selectively target T790M mutation [18,19], and were usually used for patients who had disease progression after *EGFR*-TKI treatment [20]. Even with the AZD9291 treatment, NSCLC could further gain new mutation, such as C797S or loss T790M mutation and became resistant [21]. Thus, the combination of cytotoxic chemotherapy with *EGFR*-TKIs is a promising strategy to control disease before further development of resistant mutations and enhance progression-free survival for patients with *EGFR*-mutated NSCLC [20].

Nanotechnology had revealed their advantages in specific drug delivery toward the cancer sites via the enhanced permeability and retention effects and thus fits well with the modern theme of precision medicine [22]. Our groups previously reported a well-defined, reversible disulfide cross-linked micellar (DCM) delivery system [23]. DCM was synthesized by self-assembly of a thiolated PEG-based cholic acid telodendrimer, followed by the oxidization of thiol groups to intramicellar disulfide cross-linkages. The disulfide cross-linkages could be cleaved under the intracellular reductive conditions, such as glutathione (GSH) for stimuli-responsively releasing the drug payloads. Thus, DCM formulation could prevent premature drug release during blood circulation and deliver high dose of drugs toward xenograft tumor sites resulting in increased therapeutic index and decreased toxicity [24]. Moreover, DCM formulations exhibited superior drug loading capacity, enhanced micellar stability, lack of hemolytic activity, prolonged *in vivo* circulation time as well as preferential tumor targeting. Therefore, in this study, taking advantage of this unique drug-delivery system, we used PEG^{5k}-Cys_4-L_8-CA_8 as a representative telodenrimer to develop DCM formulated AZD9291 and studied the combination effects and mechanisms of PTX–DCM and AZD9291–DCM *in vitro* and *in vivo*. To provide a better flexibility to test drug combination ratio and sequences for translational studies, we strategically loaded two drugs individually. The results suggest that the combination of PTX–DCM and AZD9291–DCM showed strong synergistic effects and could effectively eradicate NSCLC in a mouse xenograft model.

Materials & methods

Materials

PTX was obtained from AK Scientific Inc. (CA, USA). AZD9291 was purchased from Selleck Chemicals (TX, USA). Human lung adenocarcinoma H1975 cells were obtained from the American Type Culture Collection (MD, USA). RPMI-1640 medium was purchased from Gibco (CA, USA). MTS [3-(4,5-dimethyl- ldiazol-2-yl)-2,5 diphenyltetrazolium bromide], 1,1′-dioctadecyl-3,3,3′,3′tetramethylindodicarbocyanineperchlorate (DiD), a near-infrared fluorescent (NIRF) dye and all other chemicals were purchased from Sigma-Aldrich (MO, USA). Anti-IKBa, anti-pNF-κB, anti-pEGFR, anti-pAKt and anti-Bcl-2 antibodies were purchased from ABGENT (Santa Cruz Biotechnology, CA, USA).

Synthesis of DCMs

The thiolated telodendrimer (PEG^{5k}-Cys_4-L_8-CA_8) was synthesized via solution-phase condensation reactions from MeO-PEG^{5k}-NH_2 utilizing stepwise peptide chemistry as previously described [23].

Preparation & characterization of PTX–DCMs & AZD9291–DCMs

PTX (1 mg/ml), AZD9291 (1 mg/ml) and DiD (0.5 mg/ml), were loaded into DCM (20 mg/ml) by the solvent evaporation method [25]. The amount of drug loaded in the micelles was analyzed by HPLC (Waters). The drug loading content (DLC) and the drug-loading efficiency of PTX–DCMs and AZD9291–DCMs were calculated by the following equations: DLC (%) = $W_{\text{loaded drug}}/W_{\text{drug loaded DCMs}} \times 100\%$, drug loading efficiency (%) = $W_{\text{loaded drug}}/W_{\text{totaldrug}} \times 100\%$ [23,26]. The micelle solution was sterilized with 0.22 μm filters.

The morphology of PTX–DCMs and AZD9291–DCMs was observed on a Philips CM-120 transmission electron microscope (TEM, Amsterdam, the Netherlands). The particle size distribution and polydispersity index, and surface charge (ζ potential, mV) were measured by dynamic light scattering (DLS) instruments (Malvern, Zetasizernano series Nano-ZS, Malvern, UK).

The drug release profiles of the drug-loaded DCMs were performed using dialysis bags (MwCO 3500, Viskase, IL, USA) in a 1 l 10 mM of GSH containing phosphate-buffered saline (PBS). Aliquots from the dialysis bags were collected at the different time point and drug concentrations were determined by HPLC. Experiments were repeated at least three-times.

Cell culture, cellular uptake & *in vitro* cytotoxicity assay

H1975 cells were seeded at a density of 5×10^4 cells per well in eight-well tissue culture chamber slides (BD Biosciences, Bedford, MA, USA) overnight. Samples were treated with 50 μg/ml of DiD, DiD–DCMs, DiD–PTX–DCMs and DiD–AZD9291–DCMs. 4 hs later, the cells were washed and fixed 4% paraformaldehyde. The images were acquired using confocal laser scanning microscope (Carl Zeiss, LSM 800, Zeiss, Germany).

The cell viabilities were determined by MTS assay [27]. A total of 5000 H1975 cells were seeded in 96-well plates overnight. The cells were exposed to various concentrations of PTX, AZD9291, PTX–DCMs, AZD9291–DCMs alone for 72 h. To evaluate the effects of the drug combination in turns of sequence, the H1975 cells were treated with PTX–DCMs/AZD9291–DCMs 48 h + fresh medium 24 h; PTX–DCMs 24 h + AZD9291–DCMs 48 h; and AZD9291–DCMs 48 h + PTX–DCMs 24 h [27]. After 72 h of drug treatment, the culture medium was replaced with MTS working solutions. The absorbance at 490 nm was detected using a microplate ELISA reader (SpectraMax M2, Molecular Devices, USA). Cell viability as a percent of the untreated control for triplicate wells was calculated as follows: [(ODtreat - ODblank)/ (ODcontrol - ODblank) ×100%] of triplicate wells. At least three independent experiments were performed. We used 0.125-, 0.25-, 0.5-, one-, two- and four-fold the IC_{50} dose in PTX–DCMs and AZD9291–DCMs combination doses to calculate the combination index (CI) with CompuSyn® software (ComboSyn Inc., NJ, USA).

Flow cytometry analysis of apoptosis & cell cycle

The H1975 cells were seeded in six-well plate at a density of 1×10^6 cells per well overnight. Cells then treated with PTX–DCMs, AZD9291–DCMs at the concentrations of 0.3 and 3 μg/ml. After 24 h, cells were harvested and stained with Annexin V-FITC/propidium iodide (PI) (Pharmingen, CA, USA) in the binding buffer for 30 min in dark. Samples were analyzed by flow cytometry.

Regarding the cell cycle analysis, cells were treated as previously described. After 24 h of drug treatment, cells were harvested and fixed with cold 70% ethanol at 4°C for 24 h. Cells were treated with 100 μg/ml RNase-A (Sigma-Aldrich) followed by PI(50 μg/ml) staining before flow cytometry analysis. Cell cycle was analyzed by FlowJo. Experiments were performed in triplicate.

Western blot analysis

After treated with PTX, PTX–DCMs, AZD9291, AZD9291–DCMs, PTX–DCMs + AZD9291–DCMs, respectively, H1975 cells were harvested and lysed. A total of 25 μg of cell lysate protein was subjected to SDS-PAGE electrophoresis. After transferring to PVDF membranes (BioRad), membranes were blocked and incubated with the primary antibodies, including p-EGFR, p65 (pNF-κB), pAKt and β-actin overnight at 4°C followed by the peroxidase-conjugated secondary antibody (1:4000 dilution, GE Healthcare Bioscience, Belgium). Membranes were developed with Super Signal West Dura Extended Duration Substrate (Pierce Biotechnology, IL, USA) and detected by Quantity One (BioRad). Each experiment was performed at least three-times.

In vivo animal studies

In vivo NIRF optical imaging

All animal studies were performed in compliance of to UC Davis Institutional Animal Care and Use Committee (IACUC) protocols. A total of 5×10^6 H1975 cells were subcutaneously implanted on to the flank of female athymic nude mice (6–8 weeks old) (Harlan, IN, USA). After injected DiD–AZD9291–DCMs, whole mouse imaging was acquired at different time-points with Kodak multimodal imaging system IS2000MM. 48 hs later, animals were euthanized and tumors and major organs were excised and imaged.

In vivo therapeutic study

H1975 tumor-bearing mice were used for the therapeutic study. After tumor reached 100–200 mm^3, mice were randomly assigned into five groups: PBS control, free PTX (10 mg/kg), PTX–DCMs (10 mg/kg), AZD9291–DCMs (0.5 mg/kg) and the combination of PTX–DCMs (10 mg/kg) with AZD9291–DCMs (0.5 mg/kg). Free AZD9291 (0.5 mg/kg) was given via gavage every day and other groups received intravenous injection every 3 days. Of note, the stock solution for free PTX and AZD9291 was prepared in Cremophor EL and DMSO, respectively. The formulation was further diluted in PBS before each dosing. The PTX dose was chosen based on maximum tolerated dose [28], while AZD9291 dose was selected based on prior study [18]. Animal conditions were monitored daily and body weight and tumor size were measured twice a week. Tumor volume was calculated by the formula

(length × width^2)/2. Relative tumor volume equals the tumor volume at given time point divided by the tumor volume before initial treatment. One week after the last dose, blood samples were obtained for complete blood count and serum biochemistry evaluations.

Statistical analysis

Statistical analysis was performed by Student's *t*-test for two groups, and one-way analysis of variance (ANOVA) for multiple groups. All results were expressed as the mean ± standard error (SEM) unless otherwise noted. A value of $p < 0.05$ was considered statistically significant.

Result

Characterization of drug–DCMs

The results from ^{1}H NMR and MALDI-ToF MS spectra demonstrated that the thiolated telodendrimer (PEG^{5k}-Cys$_4$-L$_8$-CA$_8$) were successfully synthesized (Supplementary Figures 1–3). Both PTX and AZD9291 could be successfully loaded into DCM and the size of both nanoparticles was very small with a narrow distribution. Specifically, the diameters of PTX–DCMs and AZD9291–DCMs were 25 ± 7 nm and 19 ± 8 nm analyzed by DLS (Figure 1A), respectively. The actual size measured under TEM (Figure 1B) was consistent with the DLS findings. The polydispersity indices of PTX–DCMs and AZD9291–DCMs were 0.19 ± 0.05 and 0.18 ± 0.04, respectively. TEM results confirmed that the morphology of these drugs loaded with nanoparticles was in uniformed spherical shape with the size consistent with the DLS results. The drug loading efficiencies for PTX and AZD9291 in DCMs were 82.5 and 83.7%, while the DLCs were 16.1 and 14.3%(w/w), respectively.

Cell uptake

NCI-H1975 is T790M-positive cell line that harbors the *EGFR* L858R/T790M double mutation [29] and thus was used to study AZD9291–DCM. The cellular uptake of PTX- and AZD9291-loaded DCMs were assessed with confocal laser scanning microscope. H1975 lung adenocarcinoma cells were incubated with DiD–drug-co-loaded DCM for 2 h. As shown in Figure 2, DiD–PTX–DCMs and DiD–AZD9291–DCMs treated cells that all contained DiD signals mainly in the cytoplasm with a discrete spotty pattern. These results suggested that drug-loaded DCM could effectively internalize into H1975 cells.

In vitro effects on apoptosis & cell cycle

After confirming cellular uptake of the drug-loaded DCM, we evaluated whether loaded drug remained their anticancer activities. Cell apoptosis and cell cycle of H1975 cells after treated with different concentrations of both free and nanoformulated PTX and AZD9291 were evaluated by flow cytometry. Through apoptosis analysis, both PTX/AZD9291 and PTX–DCM/AZD9291–DCM were found to induce a dose-dependent apoptosis (Figure 3A & B, respectively) with similar dose-effects. Moreover, PTX has been shown to be related to block mitosis and resulting in cell cycle arrest at the G2/M phase. As expected, both PTX and PTX–DCM caused significant G2/M phase arrest at both 0.3 and 3 μg/ml, compared with PBS control (Figure 4A). In contrast, both AZD9291 and AZD9291–DCM treatment led to a significant G0/G1 arrest at both 0.3 and 3 μg/ml (Figure 4B). Collectively, nanoformulated drugs still remained their activity at comparable efficacies and could induce cell cycle arrest resulting in apoptosis in a dose-dependent manner.

Synergistic anti-lung cancer effect with PTX–DCM & AZD9291–DCM

Next, we intended to investigate the drug–DCM combination effects against NSCLC cells. A dose-dependent cell killing pattern was identified in all groups (Figure 5A). In agreement with the cell apoptosis and cell cycle results, PTX–DCM and AZD9291–DCM had a similar cell killing effect and comparable IC$_{50}$ against H1975 cell line (IC$_{50}$: 32.6 vs 35.3 μg/ml for PTX/PTX–DCM; IC$_{50}$: 2.13 vs 2.31 μg/ml for AZD9291/AZD9291–DCM) (Figure 5A). These results were consistent with the cell cycle/apoptosis studies and further confirmed that the drug in the uptake DCM formulations could be released to execute their cell-killing effect.

To evaluate the benefit in a combination of nanoformulated PTX and AZD9291 in the management of lung cancers, we treated H1975 cells with different concentrations of PTX–DCMs and AZD9291–DCMs as indicated. To better interpret the results, the CI was calculated with CompuSyn and we found that combination PTX–DCMs with three different concentrations of AZD9291–DCMs have synergistic effects (Figure 5B & C) evidenced by the CI less than 0.7 (Figure 5D). Additionally, western blot was performed to further elucidate the potential molecular

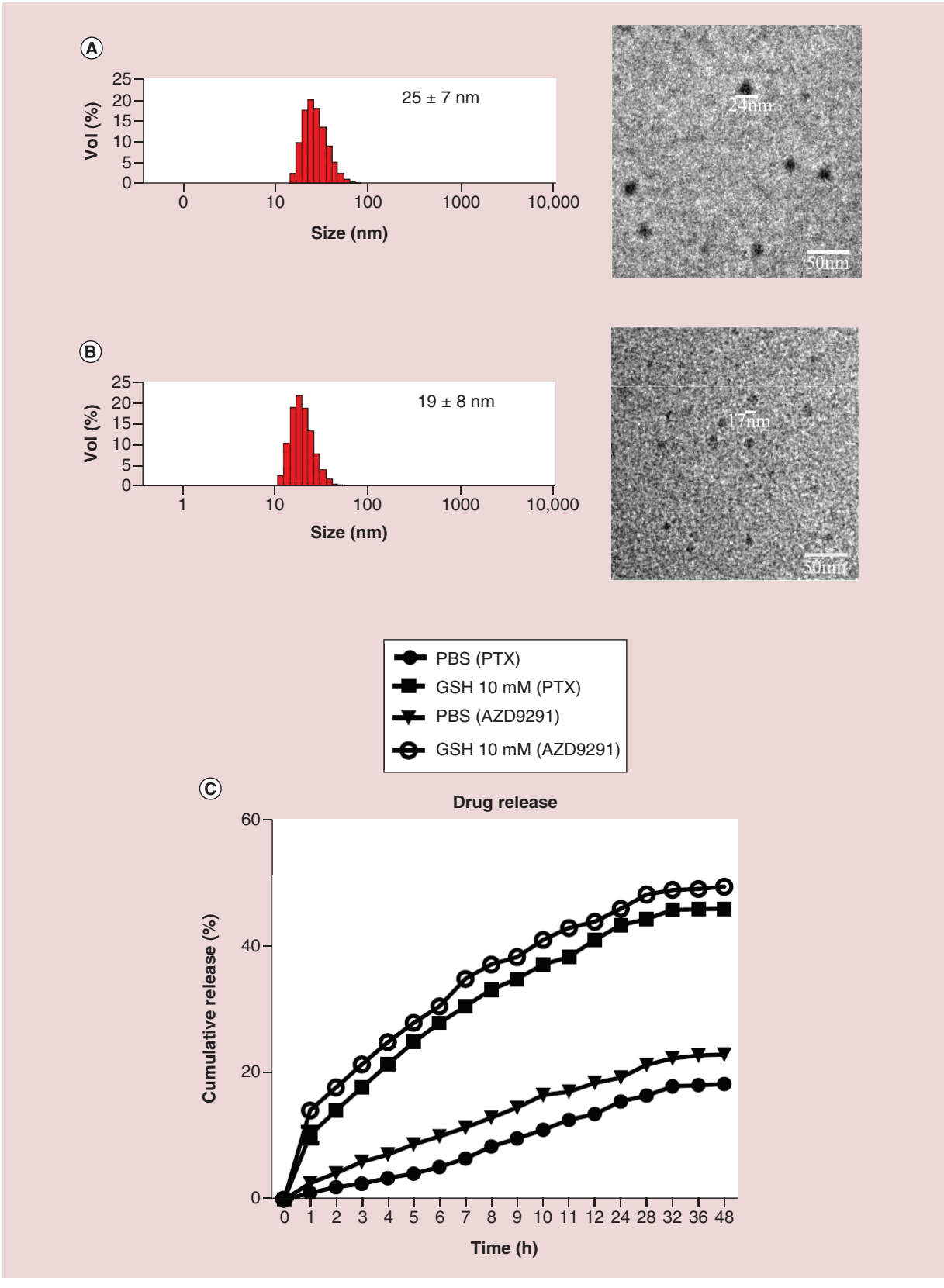

Figure 1. The physical properties of the drug-loaded nanoparticles. Characterization of PTX–disulfide cross-linking micelles (DCMs) **(A)** and AZD9291–DCMs **(B)**. (Left) Nanoparticle size and distribution were analyzed with dynamic light scattering (DLS). (Right) Transmission electron microscopy (TEM) images demonstrated the spherically shaped nanoparticles. The size observed by TEM was consistent with DLS results. Bar = 50 nm. **(C)** Drug release profiles of PTX–DCMs and AZD9291–DCMs with or without GSH at 10 mM in PBS.
GSH: Glutathione; PBS: Phosphate-buffered saline; PTX: Paclitaxel.

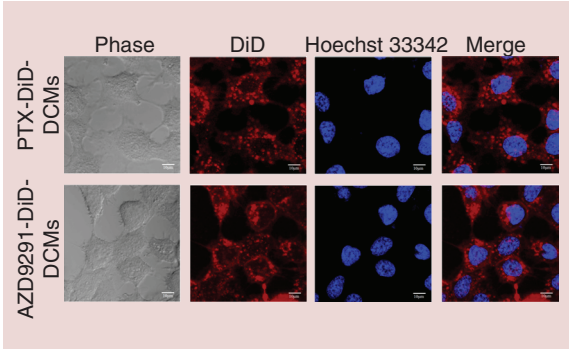

Figure 2. Intracellular delivery of PTX–DCMs and AZD9291–DCMs. Uptake of DiD (red)/drug co-loaded disulfide cross-linking micelles in lung adenocarcinoma H1975 cell lines. Cells were cultured in the eight-well chamber slides with cover glass overnight. Imaging was acquired at 2 h after incubation with DiD/drug-disulfide cross-linking micelles using confocal laser scanning microscope. Hoechst 33342 (blue) was used for nucleus staining (Scale bar = 10 μm).
DCMs: Disulfide cross-linking micelles; DiD: 1,1′-dioctadecyl-3,3,3′,3′tetramethylindodicarbocyanineperchlorate; PTX: Paclitaxel.

mechanisms for this drug combination against H1975 cell line. We evaluated several key molecules in cell signaling pathways. When treated with PTX and PTX–DCM, the expression anti-apoptotic associated molecules, *IKBa* and *Bcl-2* were decreased, *p65* (*NF-kB*) was increased, these PTX-treatment-induced decreases and increases were enhanced when cotreated with AZD9291–DCMs (Figure 5E & F). Moreover, with AZD9291 and AZD9291–DCM treatment, the phosphorylation of *EGFR* and AKT were both significantly declined (Figure 5E & F). When treated with the combination of AZD9291–DCM and PTX–DCM, it does not show significant change (Figure 5E & F).

In vivo biodistribution of AZD9291–DCMs

As previously discussed, nanoparticles could specifically accumulate at the tumor sites via enhanced permeability and retention effect. We had previously shown that PTX–DCM could passively accumulate at the SKOV-3 ovarian cancer xenografts in the mouse model [23]. In this work, we further investigated whether AZD9291–DCMs could also be delivered to the H1975 xenografts in nude mice. For this purpose, DiD, the NIRF dye also coloaded with the drug as an indicator. After intravenous injection, the signals of DiD gradually accumulated at the tumor site as early as 2 h. The high contrast of fluorescence signal between tumor and normal tissue sustained up to at least 24 h (Figure 6A). *Ex vivo* imaging at 24 h post injection further confirmed the preferential uptake of DCMs in tumor compared with that in normal organs especially lung, liver and spleen (Figure 6A). This result again confirmed the excellent capability for tumor-targeted delivery of payload with DCM platform.

In vivo therapeutic efficacy & toxicity in H1975 cancer xenograft models

The *in vivo* anticancer activity of AZD9291–DCMs was evaluated in the xenograft model of H1975 cancer. Tumor-bearing mice were administered intravenously with PBS control, free PTX (10 mg/kg), PTX–DCMs (10 mg/kg), free AZD9291 (0.5 mg/kg), AZD9291–DCMs (0.5 mg/kg) or the combination of PTX–DCMs (10 mg/kg) with AZD9291–DCMs (0.5 mg/kg), respectively, every 3 days. The free AZD9291 (0.5 mg/kg) was given via gavage every day. The relative tumor volume and body weight were measured twice per week and the results manifested that the tumor growth rate in PTX–DCMs group and AZD9291–DCMs group were inferior to free PTX group and free AZD9291 ($p < 0.05$), respectively. PTX–DCMs and AZD9291–DCMs combination almost completely suppressed tumor growth and were significantly more potent than single treatments with PTX–DCMs and AZD9291–DCMs ($p < 0.05$) (Figure 6B). As shown in Figure 6C, all the treatment caused a significant inhibition in tumor growth as compared with the PBS control ($p < 0.05$). Furthermore, the combination of PTX–DCMs with AZD9291–DCMs exerted strong synergy in tumor growth inhibition, when compared with each treatment alone ($p < 0.05$).

There were no general toxicities were noted in all groups, as all groups showed a slightly steady increase in body weight without significant difference (Figure 6B right) and all liver/kidney function parameters were within normal limits (Table 1). Consistent with our prior findings [30], complete blood count analysis showed free drug form of PTX significantly inhibited WBC counts, compared with PBS, PTX–DCMs, and combination group (Table 2). Although not significant, there was also a similar trend in RBC and hemoglobin concentration. These results indicated superior hematological toxicity profile of PTX–DCMs.

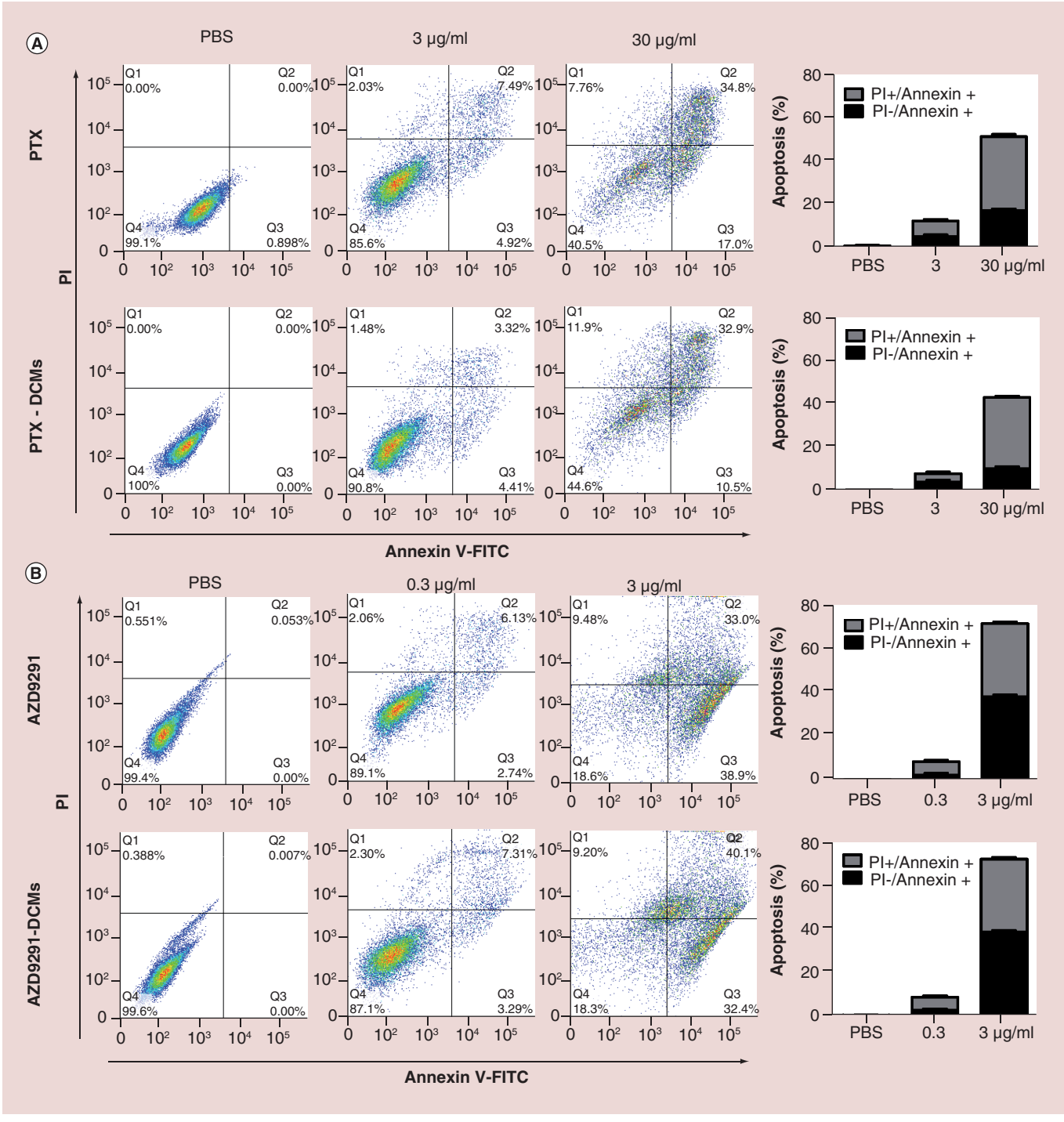

Figure 3. Flow cytometry analysis of the apoptosis of H1975 cells treated with the drug-loaded nanoparticles. Cell apoptosis analysis for H1975 cells treated with free and DCM-formulated PTX **(A)** and AZD9291 **(B)**. H1975 cells were treated with free PTX, PTX–DCMs (3 or 30 μg/ml), free AZD9291 and AZD9291–DCMs (0.3 or 3 μg/ml) for 24 h. Cells were then harvested and stained with Annexin V-FITC and propidium iodide followed by flow cytometry analysis. The left dot-plots were the representative results, while the histogram was a summary from three independent studies.
DCM: Disulfide cross-linking micelle; FITC: Fluorescein isothiocyanate; PBS: Phosphate-buffered saline; PI: Propidium iodide; PTX: Paclitaxel.

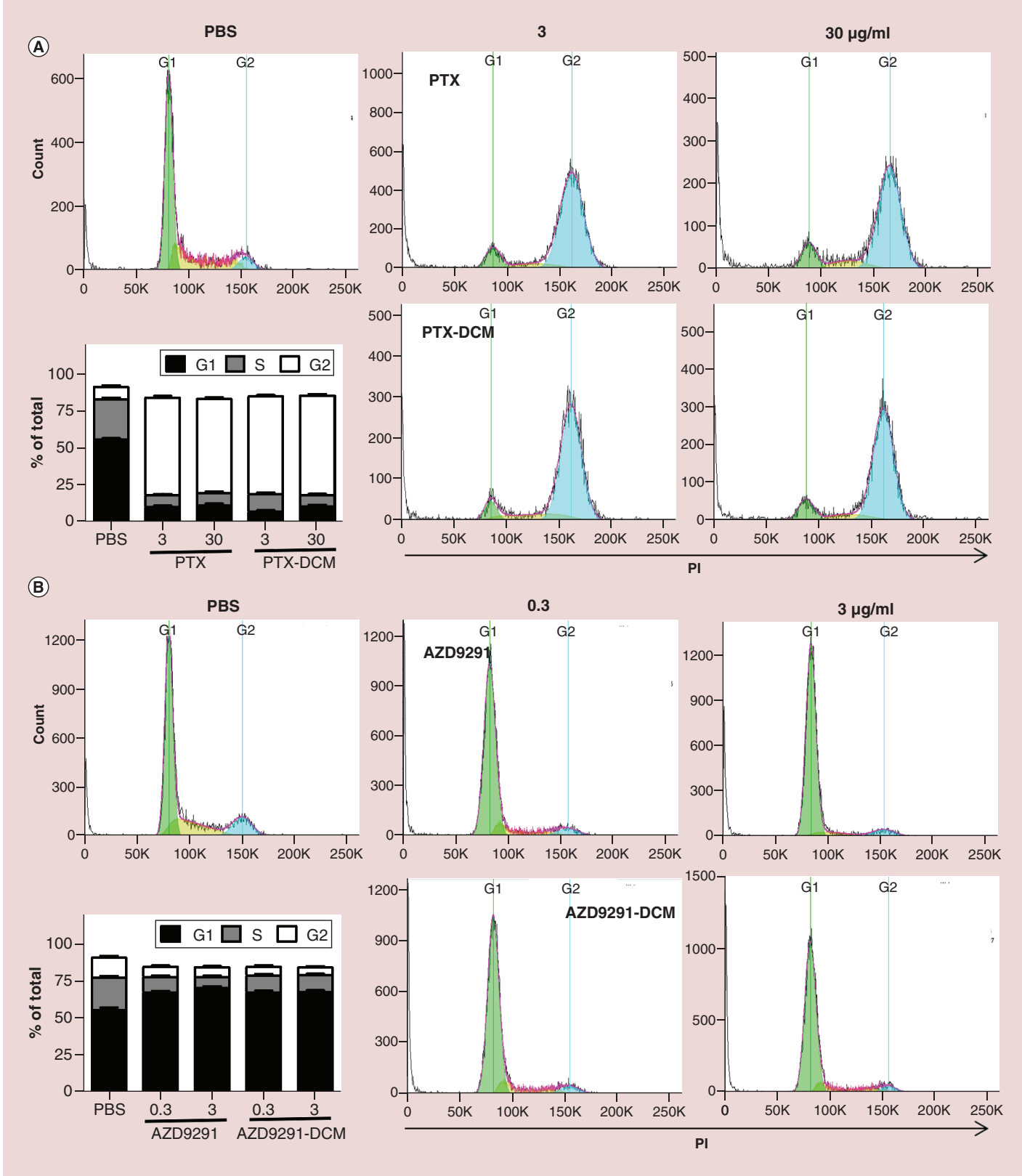

Figure 4. Cell cycle analysis of H1975 cells treated the drug-loaded nanoparticles. Cell cycle analysis for H1975 cells treated with free- and DCM-formulated PTX **(A)** and AZD9291 **(B)**, respectively. H1975 cells were treated with free PTX, PTX–DCMs (3 or 30 μg/ml), free AZD9291, and AZD9291–DCMS (0.3 or 3 μg/ml) for 24 h for flow cytometry analysis. Flow-Jo was used to perform cell cycle analysis. The histograms were the representative results, while the figure in the left-lower was the average from three independent studies. Compared with control, free PTX and PTX–DCMs (3 or 30 μg/ml) caused significant G2/M phase arrest, while free AZD9291 and AZD9291–DCMs (0.3 or 3 μg/ml) caused significant G0/G1 phase arrest. Lower-left: a summary figure from three independent studies.
DCM: Disulfide cross-linking micelle; PBS: Phosphate-buffered saline; PTX: Paclitaxel.

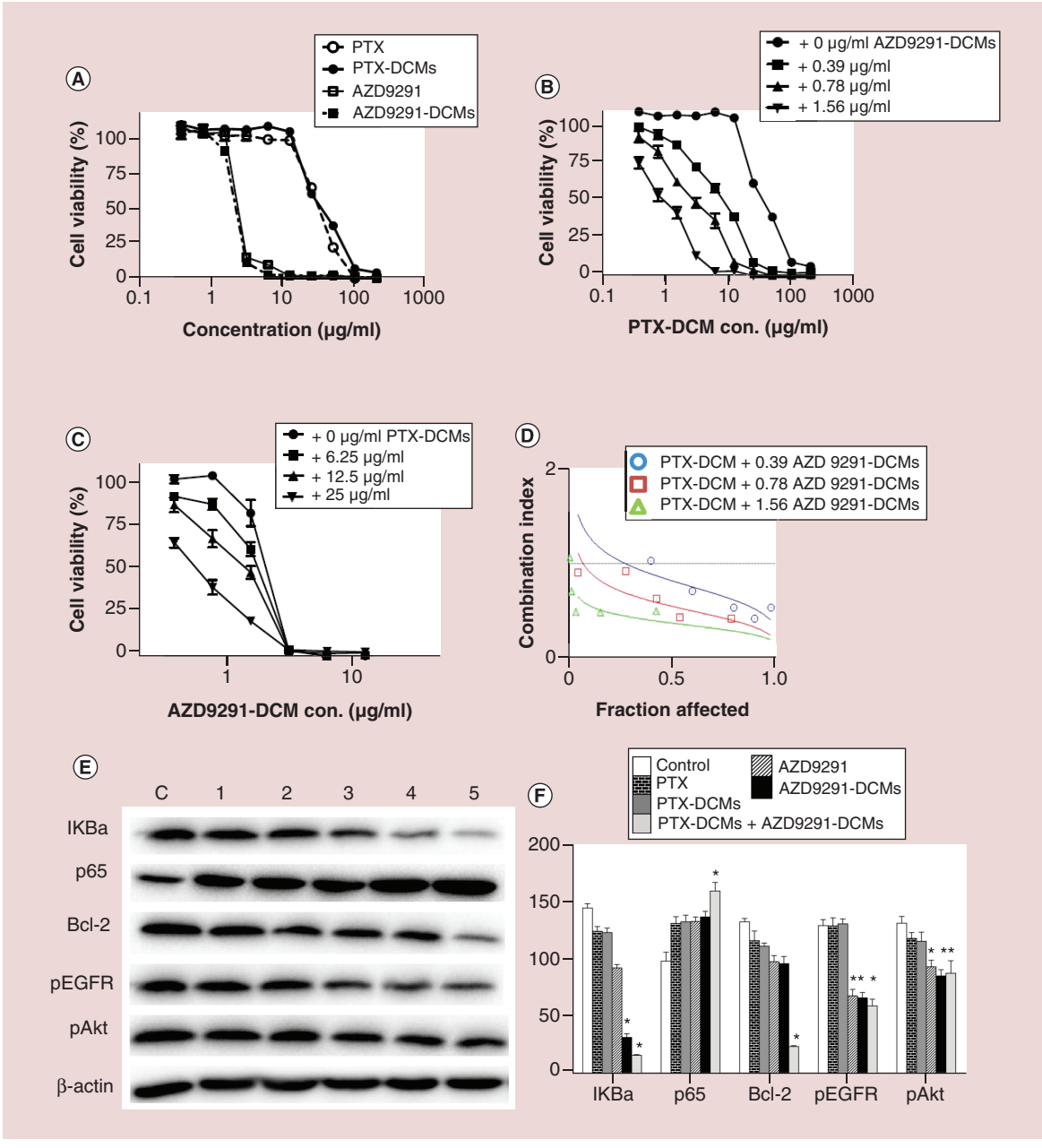

Figure 5. ***In vitro*** **anti-cancer efficacy and molecular mechanism study with PTX–DCMs, AZD9291–DCMs and combination of two nanoformulations. (A)** Cell viability study of H1975 cells after 72-h incubation with different concentrations of free drug or drug–DCMs. **(B)** Cell viability study of H1975 cells after 72-h incubation with different concentration of PTX–DCMs with 0, 0.39, 0.78 and 1.56 μg/ml of AZD9291–DCMS. **(C)** Cell viability study of H1975 cells after 72-h incubation with different concentration of AZD9291–DCMs with 0, 6.25, 12.5 and 25 μg/ml of PTX–DCMs. **(D)** Combination Index versus fraction-affected plot calculated based on the results in **(A)** and **(B)**. The results were generated with CompuSyn software. **(E)** Western blot analysis for molecular changes (*pIKK-β, p65, Bcl-xl, pEGFR, pAkt, β-actin*) at 24 h post drug treatment ([1] PTX and [2] PTX–DCM: 30 μg/ml; [3] AZD9291/[4] AZD9291–DCMs: 3 μg/ml; [5] PTX–DCMs + AZD9291–DCMs: 30 + 3 μg/ml). **(F)** Quantitative analysis of the Western blot results. β-actin was used as the loading control for each sample. $^{*}p < 0.05$.
DCM: Disulfide cross-linking micelle; PTX: Paclitaxel.

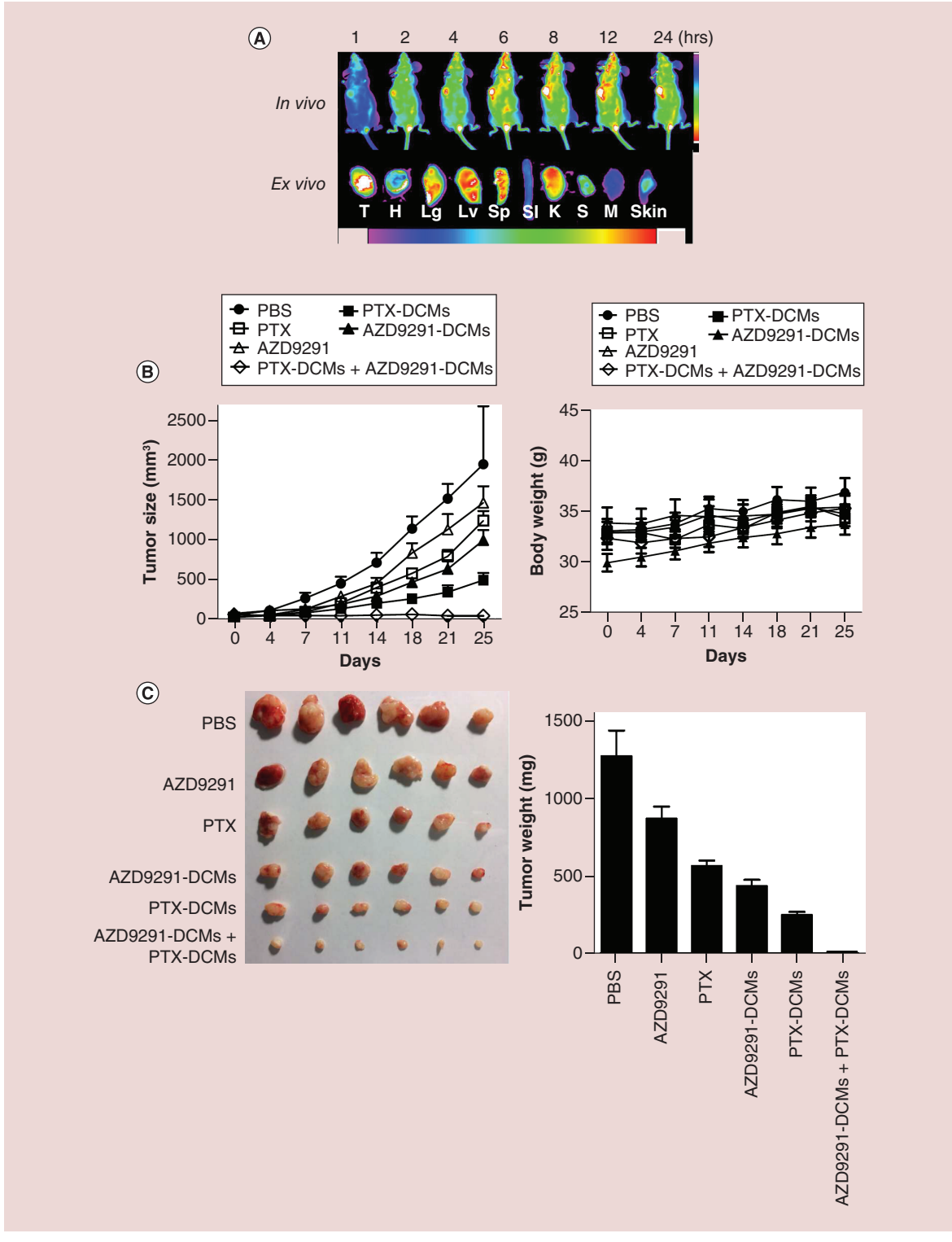

Figure 6. The synergistic therapeutic efficacy of PTX–DCMs and AZD9291–DCMs in the H1975 lung cancer xenograft model. (A) *In vivo* and *ex vivo* biodistribution of DiD/AZD9291–DCMs in H1975 lung cancer bearing mice. After a single dose of tail-vein injection (DiD: 0.1 mg/kg; AZD9291 1.0 mg/kg), near-infrared fluorescent imaging was acquired at different time points. 24 hs post injection, mice were terminated and tumor/major organs were harvested for imaging. **(B)** Tumor growth ratio curve (Left) and body weight changes (Right) of tumor bearing mice treated with free PTX (10 mg/kg), PTX–DCMs (10 mg/kg), AZD9291–DCMs (0.5 mg/kg), or the combination every 3 days for a total of six doses (dot lines). Free AZD9291 (0.5 mg/kg) was given gavage every day for a total of 15 days. Data represent mean ± standard error of the mean (n = 8–12 target lesions). *$p < 0.05$. **(C)** Real tumors pictures (Left) and weight (Right) obtained on day 25 after treatment. Bar = 1 cm.
DCM: Disulfide cross-linking micelle; DiD: 1,1′-dioctadecyl-3,3,3′,3′tetramethylindodicarbocyanineperchlorate; PBS: Phosphate-buffered saline; PTX: Paclitaxel.

Table 1. The liver and kidney functional test of H1975 xenograft bearing mice treated with paclitaxel, paclitaxel–disulfide cross-linking micelle, AZD9291, AZD9291–disulfide cross-linking micelle and the combination (n = 3).

Treatment groups	ALT (U/l)	AST (U/l)	BUN (mg/dl)	Creatinine (mg/dl)	Total bilirubin (mg/dl)
PBS	59.1 ± 9.8	160.8 ± 20.3	26.4 ± 5.6	0.13 ± 0.003	0.07 ± 0.03
PTX	33.8 ± 7.8	100.9 ± 16.8	18.8 ± 2.5	0.09 ± 0.001	0.04 ± 0.01
PTX–DCM	56.8 ± 8.3	141.9 ± 40.9	24.9 ± 1.6	0.12 ± 0.002	0.05 ± 0.02
AZD9291	34.5 ± 7.5	150.9 ± 20.9	26.2 ± 1.9	0.13 ± 0.002	0.07 ± 0.02
AZD9291–DCM	37.7 ± 5.3	116.7 ± 36.8	25.8 ± 0.7	0.12 ± 0.002	0.04 ± 0.02
PTX–DCM + AZD9291–DCM	42.8 ± 5.2	122.2 ± 29.8	21.2 ± 0.8	0.09 ± 0.003	0.06 ± 0.02

BUN: Blood urea nitrogen; DCM: Disulfide cross-linking micelle; PBS: Phosphate-buffered saline; PTX: Paclitaxel.

Table 2. The complete blood count analysis of H1975 xenograft bearing mice treated with paclitaxel, paclitaxel–disulfide cross-linking micelle, AZD9291, AZD9291–disulfide cross-linking micelle and the combination (n = 3).

Treatment groups	WBC (K/μl)	RBC (M/μl)	Hematocrit (%)	Hemoglobin (g/dl)	Platelets (K/μl)
PBS	7.1 ± 1.8	8.4 ± 2.4	41.9 ± 9.3	10.3 ± 2.5	995 ± 35
PTX	2.1 ± 0.8†	5.7 ± 0.7	33.1 ± 6.8	9.2 ± 1.6	793 ± 34
PTX–DCM	5.9 ± 0.2	7.8 ± 0.2	44.4 ± 3.1	12.5 ± 0.1	944 ± 36
AZD9291	5.2 ± 0.9	8.4 ± 0.5	38.9 ± 1.2	13.4 ± 0.3	875 ± 42
AZD9291–DCM	9.4 ± 1.6	8.8 ± 0.7	38.1 ± 7.1	12.2 ± 0.5	857 ± 34
PTX–DCM + AZD9291–DCM	4.8 ± 1.2	8.3 ± 0.5	35.3 ± 5.2	13.2 ± 0.3	973 ± 21

†$p < 0.05$ compared with phosphate-buffered saline.
DCM: Disulfide cross-linking micelle; PTX: Paclitaxel; RBC: Red blood cell; WBC: White blood cell.

Discussion

In order to minimize the adverse reactions and improve the bioavailability of the antineoplastic drugs, the nanotechnology applied in drug-delivery systems has been widely explored in recent years. Our group developed a highly versatile, well-characterized and biocompatible cross-linked micelle platform, that allows us to specially deliver one or multiple different chemotherapeutic drugs and small molecular inhibitors to the tumors [31]. In this study, we first showed that PTX–DCMs synergized with the new generation of EGFR-TKI against NSCLCs *in vitro* and *in vivo* and could eradicate NSCLC xenografts in mice with decreased hematological toxicity. Since both drugs are approved for clinical use, our studies have a very strong clinical relevance and could be readily translated.

PTX–DCMs and AZD9291–DCMs exhibited superior anti-NSCLC effects than their free counterparts *in vivo* (Figure 6). It was not surprising to display a comparable cell killing curve between free and nanoformulated drugs *in vitro*, as small molecules could usually quickly diffused into cells. DCM formulation greatly changed the pharmacokinetic and biodistribution of their payload [32]. As seen in Figure 6A, DCM delivered high doses of drugs into tumor cells and spare the rest of normal tissues. Excellent tumor targeting ability is due to their small size (around 20 nm, having good tumor penetration) and excellent serum stability (cross-linking strategy to prevent premature drug release). These results explained not only the superior anticancer effects but also the better toxicity profile *in vivo*.

The combined effect of PTX–DCMs and AZD9291–DCMs was demonstrated *in vitro* and *in vivo*, the results indicated that the anticancer effect of concomitant administration was higher than any other single drug, which was consistent with *in vitro*. To gain insight into the potential molecular mechanisms and signaling pathways involved in the synergistic anticancer effects in H1975 cell lines, we performed the western blotting to evaluate molecular changes upon mono or combination therapy. Consistent with prior study, PTX and PTX–DCM treatments through downregulated *IKBa*, increased the activity of *p65* (*NF-κB*) and then downregulated its regulatory target *Bcl-2* (Figure 5E & F) [33] to promote apoptosis [33–35]. When combined treatments with AZD9291–DCMs, the PTX induced downregulation of IKBa/p65/Bcl-2 was enhanced and suggested the combination of PTX and AZD9291 could make greater killing effects. Meanwhile, the expression levels of phosphorylation of *EGFR* and its downstream molecule Akt were decreased after the cells treated with AZD9291 and AZD9291–DCMs (Figure 5E & F). A

further combination of AZD9291 with PTX do further inhibit pEGFR and pAkt, which was consistent with the cell apoptosis and killing *in vitro* and *in vivo*.

Although several studies showed no benefit of combining chemotherapy with *EGFR*-TKIs due to cell cycle-specific antagonism, an appropriate drug administration sequences were required to show synergism [36,37]. For example, the sequence of cisplatin/PTX followed by icotinib could exert the most cell apoptosis and cell cycle arrest [38]. The study has demonstrated that sequential administrations of PTX followed by gefitinib resulted in the most effective cytotoxic effect [39]. In this study, we showed that the concurrent treatments of PTX–DCMs and AZD9291–DCMs exhibited synergistic effect (Figures 5 & 6), and our preliminary data also supported PTX–DCMs followed by AZD9291–DCMs are the most advantage schedule (data not shown). The follow-up study is undergoing. Although the extrapolation of *in vitro* data to the clinical setting should be considered with caution, these results may have implications for the rational development of chemotherapeutic regimens for the treatment of NSCLC in clinic.

Conclusion

In summary, we combined a molecular targeting agent, a chemotherapeutic agent with nanotechnology to create a versatile and biocompatible DCM platform to nanoformulated PTX and AZD9291 for NSCLC treatment. This nano-platform not only solved the issues in drug insolubility and toxicity but also enhanced their anticancer efficacy individually or in combination. Since both PTX and AZD9291 are approved by the US FDA, our study has a high clinical translation potential especially for those patients who have developed T790M *EGFR* mutation after the first line *EGFR*-TKI treatment.

Future prospective

The combination of targeted small molecular inhibitors with chemotherapeutic drugs in conjunction with nanotechnology provides level-up treatment strategies for precision medicine in treating NSCLC. This approach could potentially integrate the following advantages: right target, right tissue, right patients, right safety and right commercial potential [40], and thus has a high possibility of success. We expect this regimen would provide the most effective and safe option for NSCLC with T790M *EGFR* mutation in clinic, and thus enhance patients' quality of life and prolong their survival times.

Summary points

- Paclitaxel (PTX) and AZD9291 could be efficiently loaded in the disulfide cross-linked micelle (DCM) with drug loading efficiency at 82.5 and 83.7%, while the drug loading content were 16.1 and 14.3% (w/w), respectively.
- PTX–DCMs and AZD9291–DCM were both relatively small (size = 25 ± 7 nm and 19 ± 8 nm, respectively), spherical in shape and had very size narrow distribution.
- PTX–DCM and AZD9291–DCM could be effectively internalized by lung cancer cells with a cytoplasmic distribution.
- PTX–DCMs caused G2/M phase cell cycle arrest resulting in cell apoptosis, while AZD9291–DCMs caused G1 phase cell cycle arrest resulting cell apoptosis in NSCLC cell line.
- DCM could effectively deliver high dose of payload specifically to the non-small-cell lung cancer tumor sites in the xenograft mouse model.
- PTX–DCMs and AZD9291–DCMs exhibited significantly superior anti-non-small-cell lung cancer efficacy than their free counterparts in a mouse xenograft model.
- PTX–DCMs and AZD9291–DCMs synergistically inhibited T790M *EGFR* mutant bearing NSCLC xenograft model growth *in vivo*.
- PTX–DCMs induced IKBα/NF-κB/Bcl-2 downregulation (chemoresistance) were attenuated when cotreated with AZD9291–DCMs, while combination also further reduce phosphorylation of Akt contributing to more cancer cell death.

Supplementary data

To view the supplementary data that accompany this paper please visit the journal website at: www.futuremedicine.com/doi/suppl/10.2217/nnm-2017-0355

Authors' contributions

Li Yuanpei L, Xin-shuai W and Tzu-yin L conceived the idea and designed the drug-loaded nanoparticles for combination therapy. L Zhang, Xiaocen L, De-jiu K, Xiao-chen H, Xue-zhen D, Jun-qiang Y, Meng-qi Z, Yixuan H, Kit SL and She-gan G conducted experiments and analyzed the results. Xin-shuai W and Tzu-yin L drafted the manuscript and all authors commented on the manuscript. Yuanpei L and Tzu-yin L supervised the studies described in this report.

Financial & competing interests disclosure

This work was financially supported by the NIH/NCI (R01CA199668) and NIH/NICHD (R01HD086195). Yuanpei L and Kit SL are the inventors of a pending patent on reversibly cross-linked micelle systems. The remaining authors declare no competing financial interests. The authors have no other relevant affiliations or financial involvement with any organization or entity with a financial interest in or financial conflict with the subject matter or materials discussed in the manuscript apart from those disclosed.

No writing assistance was utilized in the production of this manuscript.

Ethical conduct of research

The authors state that they have obtained appropriate institutional review board approval or have followed the principles outlined in the Declaration of Helsinki for all human or animal experimental investigations. In addition, for investigations involving human subjects, informed consent has been obtained from the participants involved.

References

1 Jemal A, Bray F, Center MM, Ferlay J, Ward E, Forman D. Global cancer statistics. *CA Cancer J. Clin.* 61(2), 69–90 (2011).

2 Zhang H. Apatinib for molecular targeted therapy in tumor. *Drug Des. Dev. Ther.* 9, 6075–6081 (2015).

3 Rosell R, Carcereny E, Gervais R *et al.* Erlotinib versus standard chemotherapy as first-line treatment for European patients with advanced EGFR mutation-positive non-small-cell lung cancer (EURTAC): a multicentre, open-label, randomised Phase 3 trial. *Lancet Oncol.* 13(3), 239–246 (2012).

4 Datta S, Brunet A, Greenberg M. Cellular survival: a play in three Akts. *Genes Dev.* 13(22), 2905–2927 (1999).

5 Cantley LC. The phosphoinositide 3-kinase pathway. *Science* 296(5573), 1655–1657 (2002).

6 Da Cunha Santos G, Shepherd FA, Tsao MS. *EGFR* mutations and lung cancer. *Ann. Rev. Pathol.* 6, 49–69 (2011).

7 Gelderblom H, Verweij J, Nooter K, Sparreboom A. Cremophor EL: the drawbacks and advantages of vehicle selection for drug formulation. *Eur. J. Cancer* 37(13), 1590–1598 (2001).

8 Gazdar AF. Activating and resistance mutations of *EGFR* in non-small-cell lung cancer: role in clinical response to EGFR tyrosine kinase inhibitors. *Oncogene* 28(Suppl. 1), S24–S31 (2009).

9 Sharma SV, Bell DW, Settleman J, Haber DA. Epidermal growth factor receptor mutations in lung cancer. *Nat. Rev. Cancer* 7(3), 169–181 (2007).

10 Ren Y, Yao Y, Ma Q, Zhong D. *EGFR* gene-mutation status correlated with therapeutic decision making in lung adenocarcinoma. *Onco Targets Ther.* 8, 3017–3020 (2015).

11 Tiseo M, Bartolotti M, Gelsomino F, Bordi P. Emerging role of gefitinib in the treatment of non-small-cell lung cancer (NSCLC). *Drug Des. Devel. Ther.* 4, 81–98 (2010).

12 Zhang Q, Wang Z, Guo J *et al.* Comparison of single-agent chemotherapy and targeted therapy to first-line treatment in patients aged 80 years and older with advanced non-small-cell lung cancer. *Onco Targets Ther.* 8, 893–898 (2015).

13 Yu HA, Arcila ME, Rekhtman N *et al.* Analysis of tumor specimens at the time of acquired resistance to EGFR–TKI therapy in 155 patients with *EGFR*-mutant lung cancers. *Clin. Cancer Res.* 19(8), 2240–2247 (2013).

14 Niederst MJ, Sequist LV, Poirier JT *et al.* RB loss in resistant *EGFR*-mutant lung adenocarcinomas that transform to small-cell lung cancer. *Nat. Commun.* 6, 6377 (2015).

15 Sequist LV, Waltman BA, Dias-Santagata D *et al.* Genotypic and histological evolution of lung cancers acquiring resistance to EGFR inhibitors. *Sci. Transl. Med.* 3(75), 75ra26 (2011).

16 Pao W, Chmielecki J. Rational, biologically based treatment of *EGFR*-mutant non-small-cell lung cancer. *Nat. Rev. Cancer* 10(11), 760–774 (2010).

17 Rosell R, Carcereny E, Gervais R *et al.* Erlotinib versus standard chemotherapy as first-line treatment for European patients with advanced *EGFR* mutation-positive non-small-cell lung cancer (EURTAC): a multicentre, open-label, randomised Phase 3 trial. *Lancet Oncol.* 13(3), 239–246 (2012).

18 Cross DA, Ashton SE, Ghiorghiu S *et al.* AZD9291, an irreversible EGFR TKI, overcomes T790M-mediated resistance to EGFR inhibitors in lung cancer. *Cancer Dis.* 4(9), 1046–1061 (2014).

19 Janne PA, Yang JC, Kim DW *et al.* AZD9291 in EGFR inhibitor-resistant non-small-cell lung cancer. *N. Eng. J. Med.* 372(18), 1689–1699 (2015).

20 Takahashi K, Saito H. Is epidermal growth factor receptor tyrosine kinase inhibitor in combination with cytotoxic chemotherapy a better treatment option for patients with *EGFR*-mutated non-small-cell lung cancer? *Transl. Lung Cancer Res.* 5(1), 98–101 (2016).

21 Thress KS, Paweletz CP, Felip E *et al.* Acquired EGFR C797S mutation mediates resistance to AZD9291 in non-small-cell lung cancer harboring EGFR T790M. *Nat. Med.* 21(6), 560–562 (2015).

22 Kirtane AR, Siegel RA, Panyam J. A pharmacokinetic model for quantifying the effect of vascular permeability on the choice of drug carrier: a framework for personalized nanomedicine. *J. Pharm. Sci.* 104(3), 1174–1186 (2015).

23 Li Y, Xiao K, Luo J *et al.* Well-defined, reversible disulfide cross-linked micelles for on-demand PTX delivery. *Biomaterials* 32(27), 6633–6645 (2011).

24 Li Y, Xiao K, Zhu W, Deng W, Lam KS. Stimuli-responsive cross-linked micelles for on-demand drug delivery against cancers. *Adv. Drug Deliv. Rev.* 66, 58–73 (2014).

25 Yu S, Ding J, He C, Cao Y, Xu W, Chen X. Disulfide cross-linked polyurethane micelles as a reduction-triggered drug-delivery system for cancer therapy. *Adv. Healthc. Mater.* 3(5), 752–760 (2014).

26 Ho MY, Mackey JR. Presentation and management of docetaxel-related adverse effects in patients with breast cancer. *Cancer Manag. Res.* 6, 253–259 (2014).

27 Xiao K, Li YP, Wang C *et al.* Disulfide cross-linked micelles of novel HDAC inhibitor thailandepsin A for the treatment of breast cancer. *Biomaterials* 67, 183–193 (2015).

28 Kinoshita J, Fushida S, Tsukada T *et al.* Comparative study of the antitumor activity of Nab-paclitaxel and intraperitoneal solvent-based paclitaxel regarding peritoneal metastasis in gastric cancer. *Oncol. Rep.* 32(1), 89–96 (2014).

29 Tang ZH, Jiang XM, Guo X, Fong CM, Chen X, Lu JJ. Characterization of osimertinib (AZD9291)-resistant non-small-cell lung cancer NCI-H1975/OSIR cell line. *Oncotarget* 7(49), 81598–81610 (2016).

30 Lin TY, Li YP, Zhang H *et al.* Tumor-targeting multifunctional micelles for imaging and chemotherapy of advanced bladder cancer. *Nanomedicine* 8(8), 1239–1251 (2013).

31 Vyslouzil J, Bavolarova J, Kejdusova M, Vetchy D, Dvorackova K. Cationic Eudragit® polymers as excipients for microparticles prepared by solvent evaporation method. *Ceska Slov. Farm.* 62(6), 249–254 (2013).

32 Zhang H, Li Y, Lin TY *et al.* Nanomicelle formulation modifies the pharmacokinetic profiles and cardiac toxicity of daunorubicin. *Nanomedicine* 9(12), 1807–1820 (2014).

33 Jin X, Qiu L, Zhang D *et al.* Chemosensitization in non-small-cell lung cancer cells by IKK inhibitor occurs via NF-kappaB and mitochondrial cytochrome C cascade. *J. Cell. Mol. Med.* 13(11–12), 4596–4607 (2009).

34 Chun E, Lee KY. Bcl-2 and Bcl-xL are important for the induction of paclitaxel resistance in human hepatocellular carcinoma cells. *Biochem. Biophys. Res. Commun.* 315(3), 771–779 (2004).

35 Hunter TB, Manimala NJ, Luddy KA, Catlin T, Antonia SJ. Paclitaxel and TRAIL synergize to kill paclitaxel-resistant small cell lung cancer cells through a caspase-independent mechanism mediated through AIF. *Anticancer Res.* 31(10), 3193–3204 (2011).

36 Baselga J. Combining the anti-EGFR agent gefitinib with chemotherapy in non-small-cell lung cancer: how do we go from INTACT to impact? *J. Clin. Oncol.* 22(5), 759–761 (2004).

37 Herbst RS, Prager D, Hermann R *et al.* TRIBUTE: a Phase III trial of erlotinib hydrochloride (OSI-774) combined with carboplatin and paclitaxel chemotherapy in advanced non-small-cell lung cancer. *J. Clin. Oncol.* 23(25), 5892–5899 (2005).

38 Wang MC, Liang X, Liu ZY *et al. In vitro* synergistic antitumor efficacy of sequentially combined chemotherapy/icotinib in non-small-cell lung cancer cell lines. *Oncol. Rep.* 33(1), 239–249 (2015).

39 Cheng H, An SJ, Dong S *et al.* Molecular mechanism of the schedule-dependent synergistic interaction in *EGFR*-mutant non-small-cell lung cancer cell lines treated with paclitaxel and gefitinib. *J. Hematol. Oncol.* 4, 5 (2011).

40 Cook D, Brown D, Alexander R *et al.* Lessons learned from the fate of AstraZeneca's drug pipeline: a five-dimensional framework. *Nat. Rev. Drug Dis.* 13(6), 419–431 (2014).